Journal of Marine Systems 143 (2015) 62–72

Contents lists available at ScienceDirect

Journal of Marine Systems

journal homepage: www.elsevier.com/locate/jmarsys

Contrasting optical properties of surface waters across the Fram Strait and its potential biological implications

Alexey K. Pavlov [a,b,*], Mats A. Granskog [a], Colin A. Stedmon [c], Boris V. Ivanov [b,d], Stephen R. Hudson [a], Stig Falk-Petersen [a,e,f]

[a] Norwegian Polar Institute, Fram Centre, 9296 Tromsø, Norway
[b] Arctic and Antarctic Research Institute, 199397 St. Petersburg, Russia
[c] National Institute for Aquatic Resources, Technical University of Denmark, 2920 Charlottenlund, Denmark
[d] St. Petersburg State University, 199178 St. Petersburg, Russia
[e] Akvaplan-niva, Fram Centre, 9296 Tromsø, Norway
[f] Faculty of Biosciences, Fisheries and Economics, UiT The Arctic University of Norway, 9037 Tromsø, Norway

ARTICLE INFO

Article history:
Received 22 August 2014
Received in revised form 5 November 2014
Accepted 11 November 2014
Available online 17 November 2014

Keywords:
Colored dissolved organic matter (CDOM)
Light attenuation
Optical properties
Marine ecology
Arctic Ocean
Fram Strait

ABSTRACT

Underwater light regime is controlled by distribution and optical properties of colored dissolved organic matter (CDOM) and particulate matter. The Fram Strait is a region where two contrasting water masses are found. Polar water in the East Greenland Current (EGC) and Atlantic water in the West Spitsbergen Current (WSC) differ with regards to temperature, salinity and optical properties. We present data on absorption properties of CDOM and particles across the Fram Strait (along 79° N), comparing Polar and Atlantic surface waters in September 2009 and 2010. CDOM absorption of Polar water in the EGC was significantly higher (more than 3-fold) compared to Atlantic water in the WSC, with values of absorption coefficient, $a_{CDOM}(350)$, m^{-1} of 0.565 ± 0.100 (in 2009) and 0.458 ± 0.117 (in 2010), and 0.138 ± 0.036 (in 2009) and 0.153 ± 0.039 (in 2010), respectively. An opposite pattern was observed for particle absorption with higher absorption found in the eastern part of the Fram Strait. Average values of particle absorption ($a_P(440)$, m^{-1}) were 0.016 ± 0.013 (in 2009) and 0.014 ± 0.011 (in 2010), and 0.047 ± 0.012 (in 2009) and 0.016 ± 0.014 (in 2010), respectively for Polar and Atlantic water. Thus absorption of light in eastern part of the Fram Strait is dominated by particles — predominantly phytoplankton, and the absorption of light in the western part of the strait is dominated by CDOM, with predominantly terrigenous origin. As a result the balance between the importance of CDOM and particulates to the total absorption budget in the upper 0–10 m shifts across Fram Strait. Under water spectral irradiance profiles were generated using ECOLIGHT 5.4.1 and the results indicate that the shift in composition between dissolved and particulate material does not influence substantially the penetration of photosynthetic active radiation (PAR, 400–700 nm), but does result in notable differences in ultraviolet (UV) light penetration, with higher attenuation in the EGC. Future changes in the Arctic Ocean system will likely affect EGC through diminishing sea-ice cover and potentially increasing CDOM export due to increase in river runoff into the Arctic Ocean. Role of attenuation of light by CDOM in determining underwater light regime will become more important, with a potential for future increase in marine productivity in the area of EGC due to elevated PAR and lowered UV light exposures.

1. Introduction

The Arctic has undergone significant changes over the past decades associated primarily with a decrease in sea-ice extent, thickness and volume (AMAP, 2011; Meier et al., 2014), rising oceanic temperatures (Pavlov et al., 2013; Polyakov et al., 2005, 2011), and subsequent changes in biogeochemical cycling and marine ecosystem functioning (Falk-Petersen et al., 2000; Post et al., 2013, Wassmann et al., 2011). The quantity and quality of solar light reaching the surface of the Arctic Ocean (sea-ice or ocean), reflected and transmitted into the upper ocean are directly or indirectly linked to these transformations in the Arctic system. The most known Pan-Arctic examples would be the ice-albedo feedback mechanism (Serreze and Barry, 2011), accelerating sea-ice melt, and the fact that light limits marine primary production in the Arctic Ocean (Arrigo et al., 2008; Popova et al., 2012; Vancoppenolle et al., 2013).

In this context, knowledge of the optical properties of Arctic surface waters is key to understanding the current and future fate of the solar radiation in the surface layer of the Arctic Ocean. The observed and

* Corresponding author at: Norwegian Polar Institute, Fram Centre, N-9296 Tromsø, Norway. Tel.: +47 77750697.
E-mail address: pavlov.alexey.k@gmail.com (A.K. Pavlov).

http://dx.doi.org/10.1016/j.jmarsys.2014.11.001

projected decrease in summer sea-ice thickness and extent (Stocker et al., 2013) is exposing a larger area to direct solar light and allowing more energy to be transmitted through younger and thinner first-year ice (Hudson et al., 2013; Nicolaus et al., 2012). Several studies have already reported on enhanced solar heat trapping by organic matter absorption within upper layer (Granskog et al., 2007; Hill, 2008; Pegau, 2002) and sub-surface layer, leading to formation of the near surface temperature maximum, NSTM (Jackson et al., 2010), with potential contributions to enhanced stratification in the surface waters and enhanced bottom sea-ice melt (Perovich et al., 2014; Wang et al., 2014). From a biological perspective, elevated underwater light levels have been shown to result in increased Arctic Ocean primary productivity (Arrigo et al., 2008; Popova et al., 2012).

Light absorption in seawater is defined by the contribution of pure water itself, and inorganic and organic material, which is present in both dissolved and particulate forms. So-called colored dissolved organic matter or CDOM is an optically active fraction of dissolved organic matter (DOM). Particulate organic matter consists of living organisms and detritus. All these substances have characteristic absorption properties in the visible range of solar spectrum (e.g. Mobley, 1994), and thus defining spectral quality and quantity of underwater light. Despite their importance, the optical properties of Arctic surface waters have not been thoroughly investigated in the past owing to inaccessibility and prevalence of sea-ice in the Arctic Ocean. Recently, however, observations across the Arctic Ocean proper and over the continental shelf seas have become available (Falk-Petersen et al., 2000; Granskog, 2012; Granskog et al., 2007, 2012; Hill, 2008; Matsuoka et al., 2007, 2011, 2014; Pegau, 2002; Stedmon et al., 2011). These observations revealed some counterintuitive peculiarities in the absorption budget of the surface layer in the Arctic Ocean. Initial concepts about surface layer in the Arctic Ocean being transparent waters (Smith, 1973), were shifted towards a modern perception of the Arctic Ocean surface waters being optically more complex with a dominant absorption by CDOM of terrestrial origin (e.g. Granskog et al., 2007; Hill, 2008; Matsuoka et al., 2007; Pegau, 2002). Modeling studies suggest a likely future increase in Arctic Ocean primary productivity (Vancoppenolle et al., 2013), which could potentially alter optical properties and light availability in the upper layer. Thus, a comprehensive description of optical properties of both CDOM and particles, their distribution and contribution to light attenuation are essential for further advances in light budget in the Arctic Ocean, and its potential Arctic-wide implications.

In a recent study, Hancke et al. (2014) described the optical properties of CDOM across the Polar Front in the Barents Sea and found surprisingly little variability in its contribution to light penetration, showing apparently no contrast in optical properties between Arctic and Atlantic waters, further the material was considered to be of autochthonous (marine) origin. Opposite to the Barents Sea, Fram Strait is a region where a major outflow of Polar surface waters with high levels of terrestrial organic matter takes place (Amon, 2003; Granskog et al., 2012). With the projected increase in riverine discharge and associated input of the dissolved organic matter into the Arctic Ocean (Stocker et al., 2013), waters in the Fram Strait are expected to undergo a notable shift with regards to underwater light regime. In this study, we highlight the contrasting optical properties of waters of the Polar and Atlantic origin across the northern part of the Fram Strait and discuss potential implications for ecological studies.

2. Data and methods

2.1. Sampling area

Samples were collected during the cruises “Fram Strait 2009” and “Fram Strait 2010,” hereafter FS2009 and FS2010, respectively, of the Norwegian Polar Institute (NPI, Tromsø, Norway) onboard R/V Lance. Sampling was carried out during: 1st to 26th of September 2009 and 3rd to 18th of September 2010 (Dodd et al., 2012; Granskog et al., 2012) along a section across Fram Strait at 79° N (Fig. 1). Observations were made on 24 oceanographic stations each year, resulting in 48 stations in total.

The section spans from Kongsfjorden and the adjacent continental shelf across the warm and saline West Spitsbergen Current (WSC) propagating northward on the eastern flank and the relatively fresh and cold East Greenland Current (EGC) carrying Polar waters and sea-ice from the Arctic Ocean southwards.

2.2. Sampling and CTD observations

At each station, conductivity–temperature–depth (CTD) profiles were obtained with a calibrated Seabird SBE911plus profiler and seawater samples were collected with SBE32 Carousel Water Sampler equipped with 12 Niskin bottles (Dodd et al., 2012). Recently calibrated WET Labs ECO FL optical fluorescence sensor provided us with a data on vertical distribution of chlorophyll fluorescence (excitation and emission wavelengths are 470 and 695 nm, respectively) as a proxy of chlorophyll-a concentration (Kolber and Falkowski, 1993). For the upper 100 m layer sampling depths were 5, 10 (in 2010), 15 (in 2009), 25, 50, 75 and 100 m. Samples for salinity, CDOM absorption and particulate absorption measurements were collected from all depths, except for samples for particulate absorption in 2009 that were sampled only at 5, 15, 25, and 50 m.

Salinity samples were processed on board using a Guildline 8410A salinometer and IAPSO standard water (Dodd et al., 2012). CDOM samples were collected from Niskin bottles and were immediately syringe filtered (Pall Acrodisc® PF; 0.8/0.2 μm pore size, with Supor® membrane) into pre-combusted amber glass vials. Samples were stored in dark at +4 °C until analysis (Granskog et al., 2012).

Seawater for particulate absorption measurements was filtered through 25 mm Whatman GF/F filters with low vacuum. The volume of filtered water varied from 600 ml to 1500 ml depending on apparent chlorophyll concentration (color on the filter). After filtration, filters were placed into Petri dishes and immediately frozen at −80 °C until analysis.

2.3. Laboratory analysis: CDOM and particle absorption

Absorbance of CDOM was measured in the spectral range between 240 and 700 nm with an increment of 0.5 nm using a Shimadzu UV-2450 spectrophotometer and 100 mm quartz cells with ultrapure Milli-Q as a reference, following a procedure described in Stedmon and Markager (2001). The following spectrophotometer settings were used: slit width of 5 nm and fast scan speed. Absorbance values were baseline corrected and then converted to an absorption coefficient ($a_{CDOM}(\lambda)$ with m^{-1} as units) following Eq. (1):

$$a_{CDOM}(\lambda) = 2.303 \cdot A(\lambda)/l \quad (1)$$

where $A(\lambda)$ is the absorbance at a given wavelength λ and l is the path length of a cuvette in meters (here 0.1 m).

Spectral absorption (350–800 nm) of particulate material was assessed by means of the quantitative filter technique described by Mitchell (1990). Absorbance of all samples was measured using a Shimadzu spectrophotometer (UV-2450) equipped with an integrating sphere with similar spectrophotometer settings as for CDOM measurements: slit width of 5 nm and fast scan speed. Blank spectra of filters (prepared in the field) with Milli-Q water were subtracted. Optical density of all spectra was corrected for background attenuation by subtracting the average optical density measured between 750 and 800 nm. The particulate absorption coefficients ($a_p(\lambda)$ with m^{-1} as units) were calculated based on Eq. (2) (Staehr and Markager, 2004):

$$a_p(\lambda) = 2.303 \cdot A(\lambda) \cdot AF/(V \cdot \beta(\lambda)) \quad (2)$$

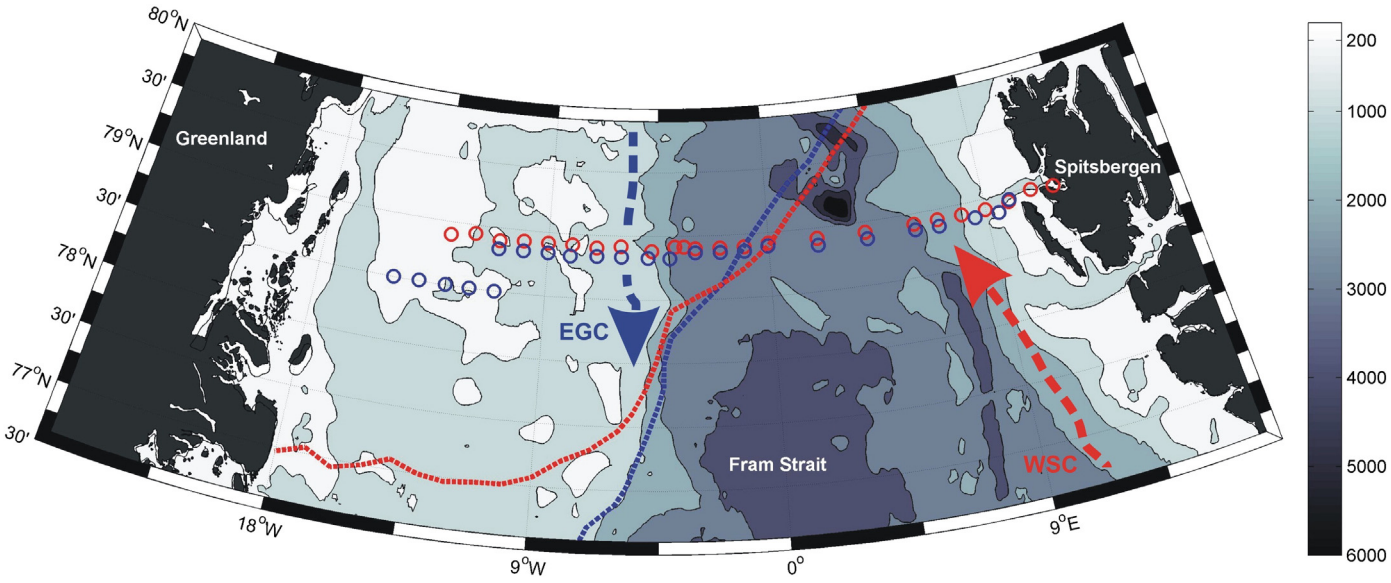

Fig. 1. Map of the study area depicting 2009 (blue) and 2010 (red) stations and average September ice edge position (dashed line, similar colors). WSC and EGC are shown schematically. Bathymetry is based on ETOPO2v2 database (U.S. Department of Commerce et al., 2006). (For interpretation of the references to color in this figure legend, the reader is referred to the web version of the article.)

where $A(\lambda)$ is the absorbance, V is the volume filtered (m^3), AF is the effective filter area (m^2) and $\beta(\lambda) = 1.63 \cdot A(\lambda)^{-0.22}$ is the β correction described in Bricaud and Stramski (1990).

2.4. Computation of underwater light field with ECOLIGHT model

For radiative transfer computations we used a certified ECOLIGHT 5.1.4 model from Sequoia Scientific Inc. (Mobley and Sundman, 2008). Pure water optical properties are taken from Pope and Fry (1997). Vertical profiles of chlorophyll a were obtained from the fluorescence sensor. Parameterization of phytoplankton scattering was done according to Loisel and Morel (1998) with a backscattering ratio, bb/b = 0.014. The model was run with a solar elevation angle of 14.3°, representative of 79° N at noon on 15 September; two setups were used for the optical properties of the water column, one corresponding to typical conditions in the WSC (6° E) and one the EGC (9° W). Incident spectral irradiance was modeled in two configurations, clear sky and overcast using a built-in RADTRAN-X subroutine of ECOLIGHT (Mobley and Sundman, 2008) with the following atmospheric parameters: average horizontal visibility of 15 km, relative humidity of 80%, and total ozone of 263.8 DU (derived from climatology incorporated in ECOLIGHT). All cases were modeled without sea ice. A comprehensive description of the model is given in a model technical documentation (Mobley and Sundman, 2008).

3. Results

3.1. Distribution of CDOM and particulate absorption in Fram Strait

The upper 100 m of our 2009 and 2010 hydrographic sections across the Fram Strait is characterized by an apparent contrast between the waters entering and exiting the Arctic Ocean in all key characteristics: T, S, $a_{CDOM}(440)$ and $a_p(440)$ (Figs. 2 and 3). Distribution of temperature and salinity (Figs. 2b and c, and 3b and c) depicts two main hydrographic features across the Fram Strait: warm and saline WSC on the eastern flank and cold and relatively fresh EGC on the western flank (Swift and Aagaard, 1981). The core of the WSC is confined to the continental slope, while the core of the EGC is more diffused and occupies the shelf to the East of Greenland. The main difference between 2009 and 2010 is the extent of the WSC. The WSC in 2009 was more pronounced compared to that in 2010, which is seen in absolute values of T and S, and in spatial extent of the core of the WSC. These observations are consistent with recent reports on the weakening of WSC after a temperature peak observed in 2006 (Walczowski et al., 2012).

Particulate absorption data covers upper 50 m in 2009 and the upper 100 m in 2010. The magnitude of $a_p(440)$ is comparable between years and the pattern is relatively similar, with highest values in the eastern part of the strait (Figs. 2d and 3d) reaching up to 0.08–0.09 m^{-1} in both years. On average, $a_p(440)$ was lower in 2009 than 2010. In 2010, the highest $a_p(440)$ is found to the east of the WSC core, in particular, close to Arctic Front, which is a zone with elevated gradients in T and S at approximately 7–9° E as well as over the West Spitsbergen shelf occupied with the Arctic waters originating from the Barents Sea (Saloranta and Svendsen, 2001). The transect in 2009 did not span as far eastwards. In the EGC area (west of 2–3° W), $a_p(440)$ was in general lower in 2009 than in 2010. In 2009, higher $a_p(440)$ values were found at the surface, while in 2010 higher $a_p(440)$ values were associated with an occasional maxima in the sub-surface layer within a depth range of 15–35 m, apparently connected to enhanced stratification layers.

Distribution of CDOM across the Fram Strait shows a distinct pattern (cf. Granskog et al., 2012), with highest $a_{CDOM}(440)$ associated with the ice covered cold EGC waters and the lowest values, sometimes close to the detection limit of the instruments, found in the core of the WSC. Distribution of $a_{CDOM}(440)$ within EGC is not homogenous; highest values were generally observed in the sub-surface layer of 30–120 m (cf. Granskog et al., 2012), while at the surface $a_{CDOM}(440)$ values are often lower. In the core of the EGC waters, $a_{CDOM}(440)$ reached up to 0.14 m^{-1}.

3.2. Relation of CDOM and particulate absorption to water masses

We used a classification using temperature and salinity of Swift and Aagaard (1981) to define water masses in the region and to look more closely into relationships between water masses and optically active substances. Two distinct water masses in the Fram Strait are Atlantic water (AW) and Polar water (PW), while remaining surface waters are various intermediate products of their mixing, and with additions from precipitation and sea-ice melt with a relatively broad temperature and salinity range. Note that originally (Swift and Aagaard, 1981) Arctic surface water (ASW) is defined as a mixing product of AW and PW, influenced by precipitation and solar heating that has a $T > 0$ °C within S range of 34.4–34.7and $T > 2$ °C for the S range of 34.7–34.9. In our

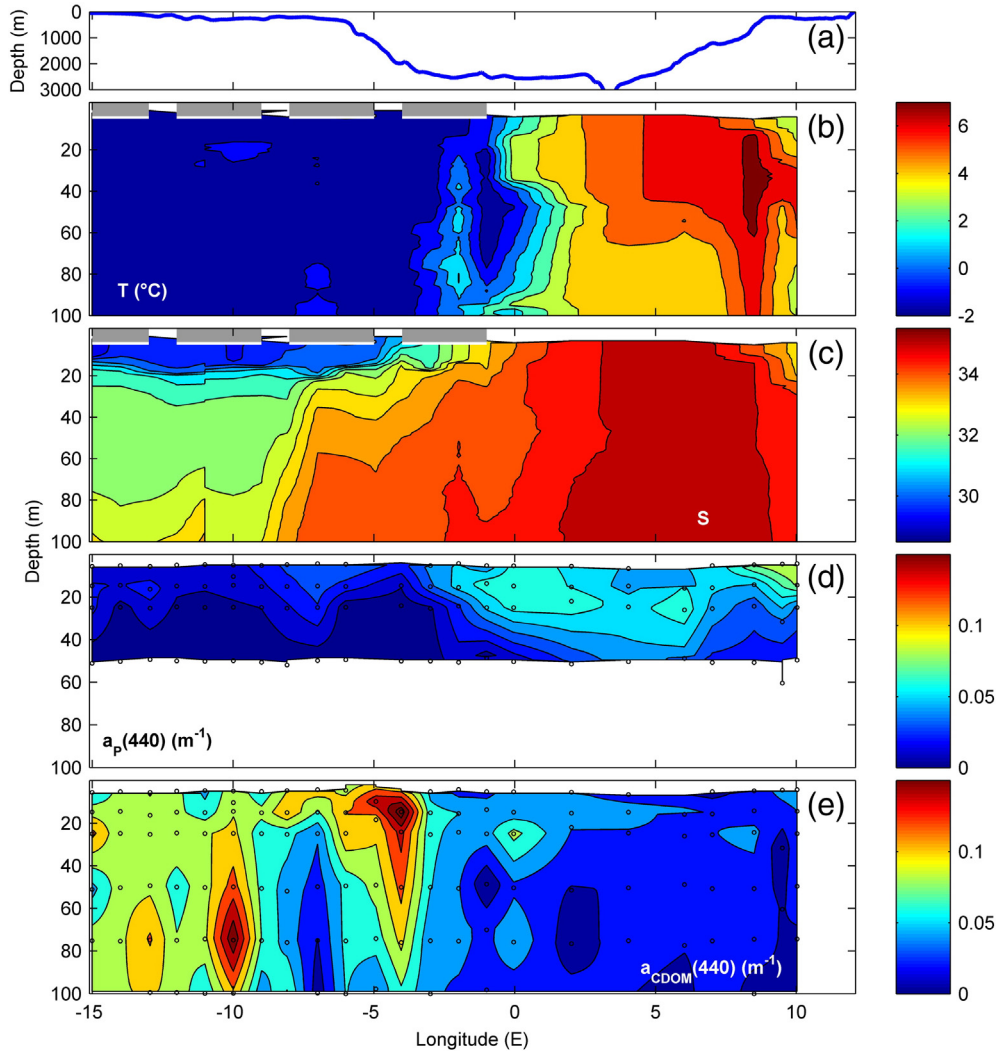

Fig. 2. Transect along 79° N in September 2009 (see Fig. 1): a) bathymetry profile, b) temperature (°C), c) salinity, d) $a_p(440)$ (m^{-1}), and e) $a_{CDOM}(440)$ (m^{-1}). Sea-ice cover at time of sampling is shown by a gray dashed line on top of subplots b) and c). Sampling depths are shown by black dots on subplots d) and e). (For interpretation of the references to color in this figure legend, the reader is referred to the web version of the article.)

study, a number of samples were found with positive temperature but fresher than 34.4. We consider those samples also as ASW, while still keeping original limits for ASW on Fig. 4 (light green dotted line) according to Swift and Aagaard (1981). In Fig. 4 we present a temperature–salinity (TS) scatter plot with $a_p(440)$ and $a_{CDOM}(350)$ as 3rd variables. Use of $a_{CDOM}(350)$ rather than $a_{CDOM}(440)$ in this graph is explained by very low CDOM absorption in the WSC introducing considerable noise into the diagram.

Highest $a_{CDOM}(350)$, up to 0.6–0.7 m^{-1}, is clearly associated with PW (cf. Granskog et al., 2012), and more precisely with waters colder than −1 °C, and salinity range of ca. 30–33. Lowest $a_{CDOM}(350)$ is found in the core of the AW as well as within ASW (Fig. 4). Lowest $a_p(440)$ values are associated with core PW as well as AW, while highest $a_p(440)$ values are found in the ASW.

3.3. Average CDOM and particulate absorption spectra within Polar and Atlantic waters

Average values of $a_{CDOM}(\lambda)$ and $a_p(\lambda)$ in different water masses were computed for the range 350–700 nm (Fig. 5). Emphasis is made on the optical properties of AW and PW, as these are the dominant surface water masses in Fram Strait. Therefore, all other water masses were grouped together and are here called remaining waters (RW), which include Arctic Surface Water (ASW), lower and upper Arctic Intermediate Waters (uAIW and lAIW) (see Fig. 4). Average $a_{CDOM}(\lambda)$ and $a_p(\lambda)$ for AW and PW at selected wavelengths that are either most often used in the literature or correspond to some of the remote sensing bands are presented in Tables 1 and 2, respectively.

CDOM absorption, $a_{CDOM}(\lambda)$, shows similar patterns for both years, being slightly higher in 2009, especially in PW. Highest $a_{CDOM}(\lambda)$ values were found within PW and lowest were found in AW as has already been indicated above (Sections 3.1 and 3.2). Mean $a_{CDOM}(\lambda)$ for RW was found to be slightly higher than for AW. Average $a_p(\lambda)$ is not as consistent between years as $a_{CDOM}(\lambda)$. Particulate absorption, $a_p(\lambda)$, was lowest in PW in both years, while $a_p(\lambda)$ for AW showed large difference from 2009 to 2010. Values of $a_p(\lambda)$ within AW in 2009 were more than twice as high as in 2010. In 2010, $a_p(\lambda)$ values within AW and PW were low and very similar. RW had the highest variation in $a_p(\lambda)$ and resulted in comparatively high average $a_p(\lambda)$ values accompanied by highest standard deviations (not shown).

3.4. Modeling underwater light distribution

To evaluate the impact of CDOM and particles on the underwater light field, we performed model simulations with ECOLIGHT 5.1.4 model (Mobley and Sundman, 2008). We selected characteristic profiles of $a_p(\lambda)$ and $a_{CDOM}(\lambda)$ taken in 2010 in the proximity of the core of the EGC (9° W) and the WSC (6° E). We assumed that no sea-ice is present

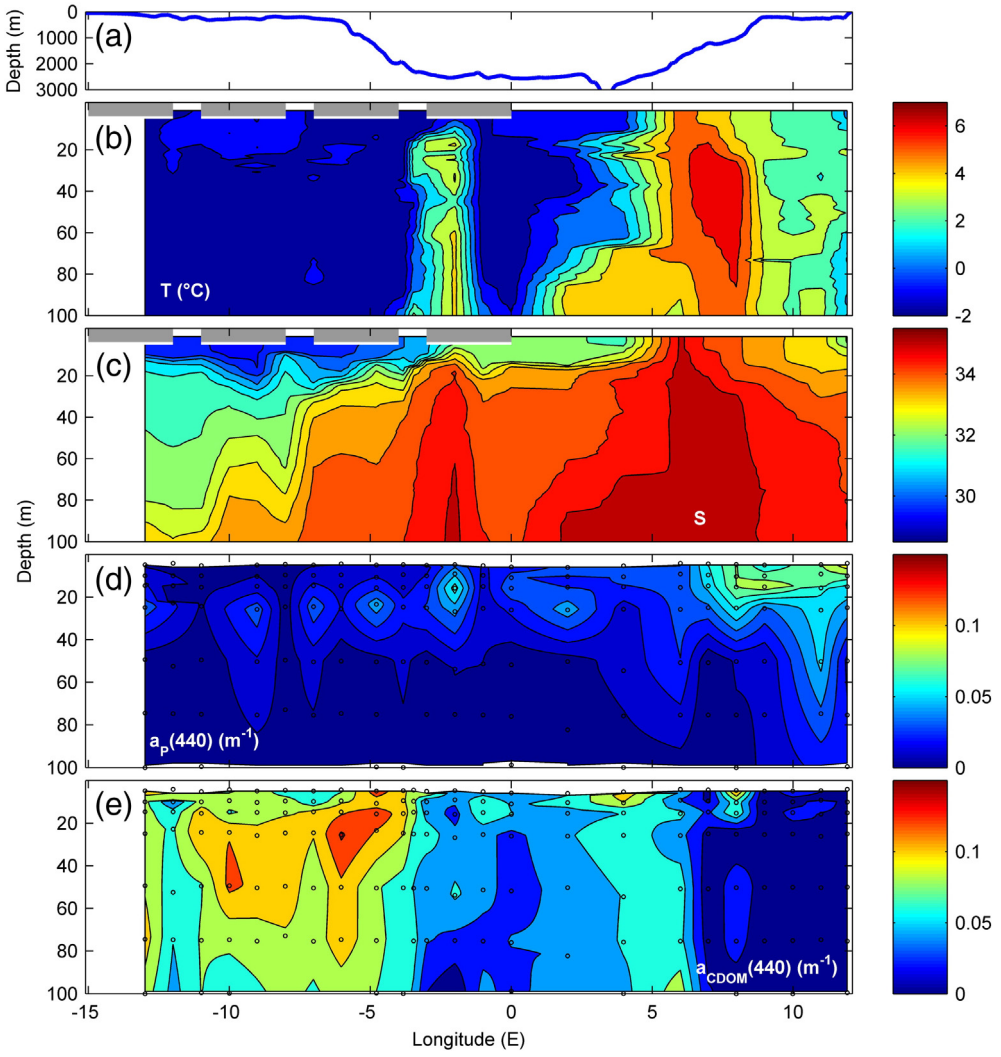

Fig. 3. Transect along 79° N in September 2010 (see Fig. 1): a) bathymetry profile, b) temperature (°C), c) salinity, d) $a_p(440)$ (m^{-1}), and e) $a_{CDOM}(440)$ (m^{-1}). Sea-ice cover is shown by a gray dashed line on top of subplots b) and c). Sampling depths are shown by black dots on subplots d) and e). (For interpretation of the references to color in this figure legend, the reader is referred to the web version of the article.)

in both cases. To facilitate comparison with a recent study in the Barents Sea by Hancke et al. (2014), ECOLIGHT 5.1.4 model was initialized similarly and similar output variables are summarized in Table 3. Graphical representation of the input data on $a_P(\lambda)$ and $a_{CDOM}(\lambda)$, modeled PAR diffuse attenuation coefficients (K_d) and modeled PAR levels are shown in Figs. 6 and 7. In contrast to Hancke et al. (2014), however, measured vertical profiles in spectral $a_P(\lambda)$ and $a_{CDOM}(\lambda)$ were assimilated into the model, rather than assuming homogenous distribution of these variables in the upper layer within AW and PW.

As pointed out in Section 4.1, CDOM absorption in the EGC was lower in the uppermost 10–15 m compared to the subsurface layer (EGC core with PW, down from 25 to 30 m). Such vertical distribution is reflected on Fig. 6, where in fact total absorption in the EGC is only slightly higher than in the WSC despite contrast in CDOM absorption between PW and AW. This results in similar K_d values in the upper 5–6 m in the EGC and WSC (Fig. 7), a layer where a substantial portion of light is attenuated. According to our calculations, under clear sky conditions, pure water and CDOM are responsible for 83% and 76% of PAR attenuation in the upper 0–10 m in the EGC and WSC, respectively, with corresponding K_d values of 0.18 m^{-1} and 0.15 m^{-1}. Corresponding euphotic zone depths are 34.1 (EGC) and 46.1 m (WSC). Pure water and particles contribute to 63% (EGC) and 81% (WSC) of the attenuated energy in top 10 m. Thus, at a first glance, contrasting optical properties in EGC and WSC do not result in substantial difference in PAR attenuation in the upper 0–10 m, 84% (EGC) and 81% (WSC) relative to the surface and with regards to euphotic depths, 31.5 (EGC) and 37.4 (WSC) respectively (Fig. 7; Table 3).

However, notable difference is observed in the UV region. Under clear sky, due to pure water and CDOM, 99% of the UV radiation is attenuated in the EGC compared to 92% in the WSC. Total attenuation in the top 10 m reaches 99% in the EGC and 93% in the WSC, with corresponding K_d values of 0.48 and 0.27 m^{-1}. As a result, 1% penetration depth in the EGC is almost half that in the WSC area, 9.6 m and 16.7 m, respectively.

4. Discussion

4.1. CDOM absorption in relation to water masses in Fram Strait

The distribution of CDOM shows a pattern closely linked to hydrography with significantly higher CDOM absorption in the EGC compared to WSC. Based on the same data set in 2009, Granskog et al. (2012) made a similar conclusion with an investigation of CDOM properties and its potential sources. Their study showed that EGC outflow carries terrestrial CDOM signature from the Arctic Ocean, probably originating from Arctic rivers. The sub-surface CDOM absorption maximum (30–120 m) in the EGC area was linked to river and sea-ice brine enriched water, characteristic of the Arctic mixed layer and upper halocline

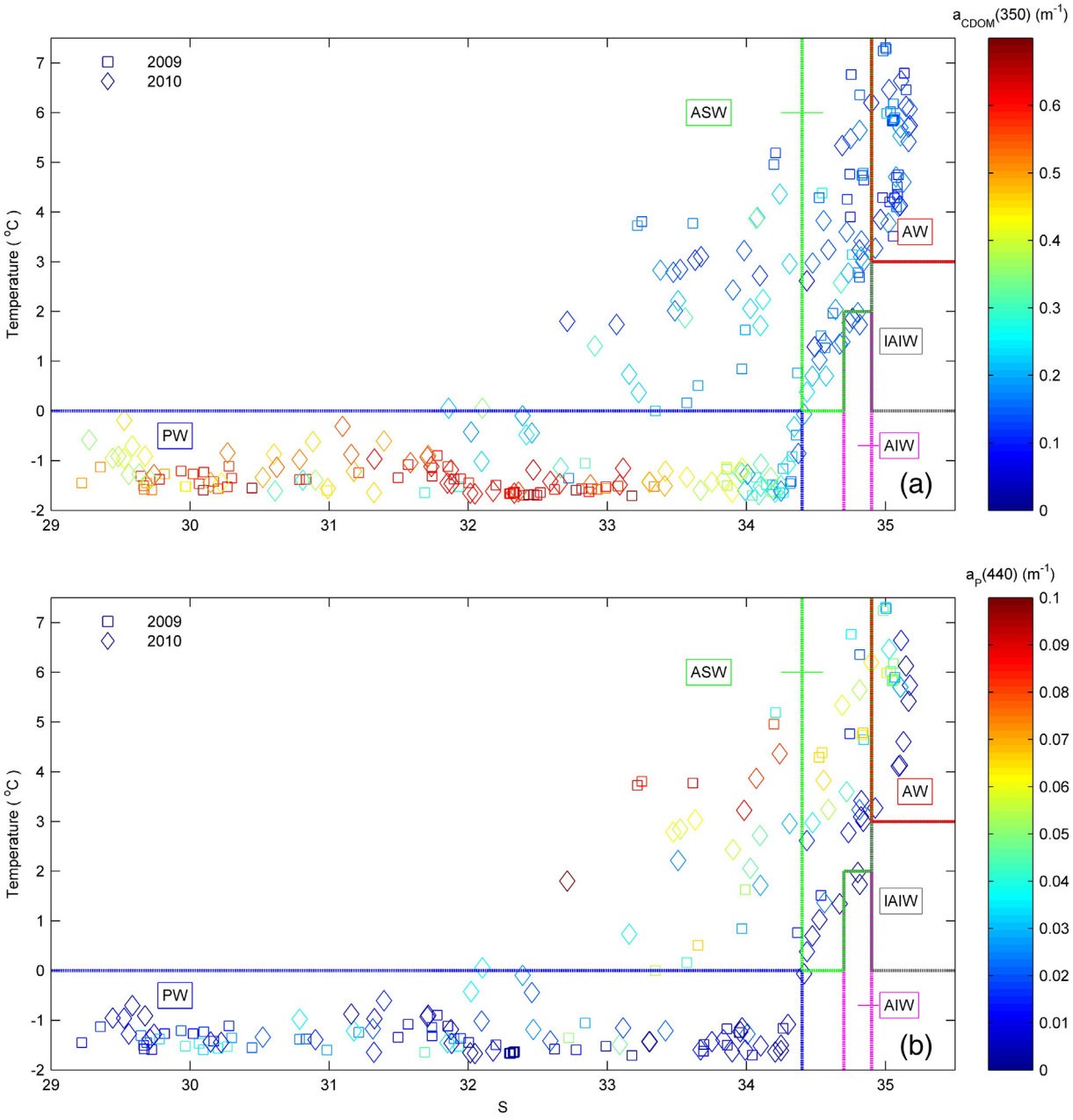

Fig. 4. TS scatter plots with a) $a_{CDOM}(350)$ as a 3rd variable (with colorbar) and b) $a_p(440)$ as a 3rd variable (with colorbar) based on data from 2009 and 2010. Water mass definitions are following Swift and Aagaard (1981). Water mass abbreviations: AW — Atlantic water, PW — Polar water, ASW — Arctic Surface water, AIW — Arctic intermediate water, lAIW — lower Arctic intermediate water. (For interpretation of the references to color in this figure legend, the reader is referred to the web version of the article.)

waters (Granskog et al., 2012) and concurs with observations of high CDOM in the EGC and surface waters of the Eurasian Basin (Amon, 2003; Stedmon et al., 2011). Lower absorption in the upper 25–30 m layer in the EGC may reflect the influence of sea-ice melt dilution and photobleaching of CDOM (Granskog et al., 2007, 2012; Pegau, 2002; Xie et al., 2014). It has been suggested that CDOM incorporated into sea ice can be lost through brine drainage in summer (Xie et al., 2014) as well as photobleaching (Belzile et al., 2000; Xie and Gosselin, 2005). Potential dilution of CDOM by sea-ice melt is then contrary to previous works in the Arctic, which suggested that CDOM accumulates in sea-ice during its formation and is subsequently released to surface waters during sea-ice melt providing a source of CDOM to the upper ocean layer (Scully and Miller, 2000). Another recent work in the Canadian Arctic (Bélanger et al., 2013) demonstrated that CDOM absorption in the upper layer affected by sea-ice melt substantially depends on the distance from terrestrial sources of CDOM (such as rivers). The presence of low CDOM layer at the surface has implications for light penetration and is further discussed in Section 4.3.

The CDOM absorption measurements in AW align with the reported values from the Polar Front region in the Barents Sea (Hancke et al., 2014). CDOM absorption is low and comparable between regions, with $a_{CDOM}(350)$ of 0.138 ± 0.036 (in 2009) and 0.153 ± 0.039 (in 2010) compared to 0.24 ± 0.07 in August 2007 in the AW of the Barents Sea (Hancke et al., 2014). Based on an empirical CDOM model (Stedmon and Markager, 2001), CDOM in AW in both Fram Strait and Barents Sea was found to be of marine origin (Granskog et al., 2012; Hancke et al., 2014). In contrast the Polar waters in the Fram Strait have higher CDOM absorption and have a greater contribution of terrestrial CDOM (Granskog et al., 2012). As a result there is more than a 3-fold difference in $a_{CDOM}(350)$, in Polar water in the EGC compared to Atlantic waters and Arctic waters in the Barents Sea. This likely reflects the differing origin of these waters with the EGC containing a contribution from

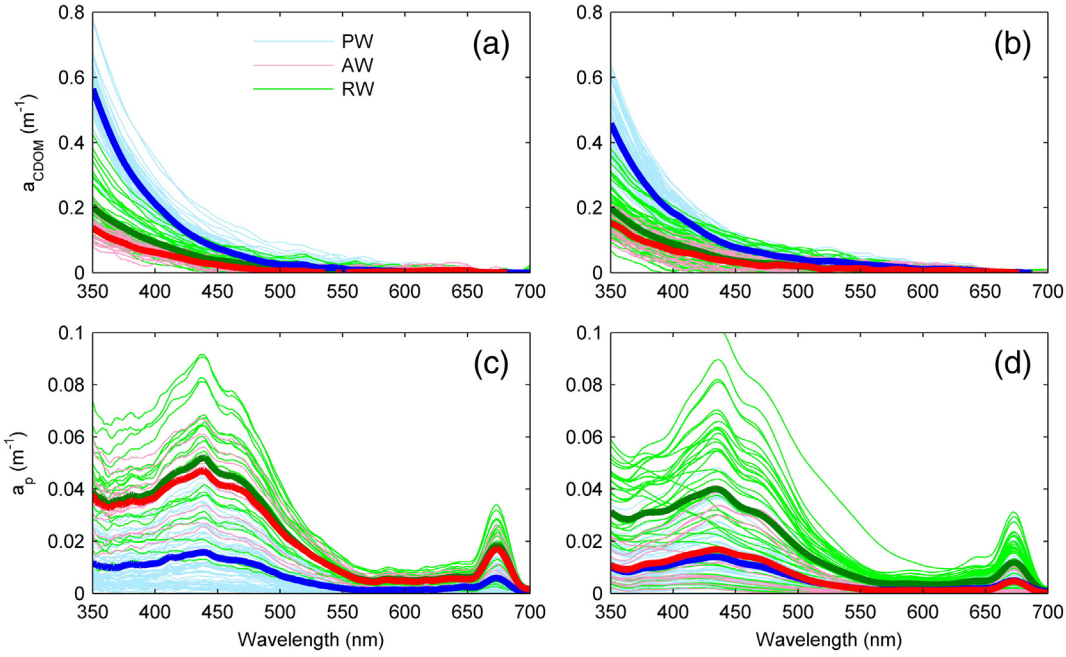

Fig. 5. A) All $a_{CDOM}(\lambda)$ spectra in 2009 and b) 2010, and c) all $a_p(\lambda)$ spectra in c) 2009 and d) 2010. Bold lines represent average spectra. Note that *Y*-axis scale is different for a), b), c), and d). (For interpretation of the references to color in this figure legend, the reader is referred to the web version of the article.)

Arctic Ocean surface and halocline waters derived from the riverine influenced shelf seas. While Barents Sea waters on both sides of the Polar Front apparently consist of waters of Atlantic origin, due to the absence of a terrestrial CDOM signal (Hancke et al., 2014), which is cooled during its transit around Svalbard and into Barents Sea. Thus, Arctic waters in the Barents Sea are different from Polar waters in the Fram Strait with regards to optical properties.

4.2. Particulate absorption in relation to water masses in Fram Strait

Despite importance for the ecosystem, upper ocean and sea-ice studies spectral absorption by particles has not been published from Fram Strait. Absorption properties by particulate matter presented in this study (September 2009 and 2010) give some insights relevant for both physical and biological studies. In the area of the WSC, high values of $a_p(440)$ to the east of the Arctic Front in 2010 (Fig. 3) are associated with the Arctic-type water over the West Spitsbergen shelf originating from the Barents Sea (Hancke et al., 2014; Saloranta and Svendsen, 2001). This can be related to enhanced coastal upwelling and mixing, and hence, additional nutrient supply to the euphotic zone stimulating phytoplankton development. In 2009 elevated $a_p(440)$ is found both to the west and east of the Arctic Front and are associated with a sharpest gradient in temperature and salinity (Fig. 2), which is likely to be a region with high biological productivity as a high latitude oceanic front (Taylor and Ferrari, 2011). Generally, the main mechanisms behind enhanced primary productivity in the front area could be explained by reduced vertical mixing (Smith et al., 1987; Sverdrup et al., 1942; Taylor and Ferrari, 2011). To the west of the Arctic Front, elevated $a_p(440)$ can also be associated with the sea-ice edge, areas generally known as a high productivity waters mostly owing to enhanced stratification in the upper layer (Taylor and Ferrari, 2011).

In the EGC area (west of 2–3° W), in 2009 $a_p(440)$ was very low with maximum values at the surface, while in 2010 $a_p(440)$ was higher than in 2009 with occasional maxima in the sub-surface layer (Figs. 2 and 3). In both years, the vertical structure of temperature and salinity was similar, with a pycnocline ranging between 15 and 35 m. The most notable difference between the 2 years was related to sea-ice conditions, with heavier ice conditions in 2009. Thus, it could cause less phytoplankton production through light limitation in the EGC area in 2009 and hence no sub-surface peaks in $a_p(440)$ were found.

Table 1
Average CDOM absorption coefficients for PW and AW.

	Polar water		Atlantic water	
	2009	2010	2009	2010
λ (nm)	Mean ± SD (m^{-1})	Mean ± SD (m^{-1})	Mean ± SD (m^{-1})	Mean ± SD (m^{-1})
320	1.033 ± 0.174	0.833 ± 0.215	0.252 ± 0.049	0.265 ± 0.049
350	0.565 ± 0.100	0.458 ± 0.117	0.138 ± 0.036	0.153 ± 0.039
355	0.512 ± 0.092	0.418 ± 0.106	0.125 ± 0.032	0.143 ± 0.038
375	0.340 ± 0.064	0.287 ± 0.072	0.091 ± 0.022	0.099 ± 0.038
400	0.212 ± 0.046	0.184 ± 0.044	0.062 ± 0.015	0.067 ± 0.032
412	0.166 ± 0.039	0.154 ± 0.036	0.053 ± 0.014	0.060 ± 0.032
440	0.092 ± 0.030	0.091 ± 0.023	0.029 ± 0.012	0.038 ± 0.027
443	0.087 ± 0.029	0.087 ± 0.022	0.028 ± 0.013	0.036 ± 0.026
490	0.031 ± 0.019	0.048 ± 0.015	0.006 ± 0.012	0.023 ± 0.022
510	0.024 ± 0.018	0.036 ± 0.012	0.005 ± 0.012	0.019 ± 0.023
555	0.009 ± 0.015	0.025 ± 0.012	0.001 ± 0.014	0.011 ± 0.019

Table 2
Average particle absorption coefficients for PW and AW.

	Polar water		Atlantic water	
	2009	2010	2009	2010
λ (nm)	Mean ± SD (m^{-1})	Mean ± SD (m^{-1})	Mean ± SD (m^{-1})	Mean ± SD (m^{-1})
350	0.011 ± 0.010	0.010 ± 0.007	0.038 ± 0.012	0.011 ± 0.007
355	0.010 ± 0.009	0.009 ± 0.007	0.034 ± 0.011	0.010 ± 0.007
375	0.011 ± 0.009	0.010 ± 0.007	0.034 ± 0.010	0.011 ± 0.007
400	0.011 ± 0.009	0.011 ± 0.009	0.037 ± 0.009	0.013 ± 0.009
412	0.014 ± 0.011	0.013 ± 0.010	0.042 ± 0.011	0.015 ± 0.011
440	0.016 ± 0.013	0.014 ± 0.011	0.047 ± 0.012	0.016 ± 0.014
443	0.015 ± 0.013	0.013 ± 0.011	0.045 ± 0.011	0.016 ± 0.014
490	0.009 ± 0.008	0.007 ± 0.006	0.030 ± 0.008	0.009 ± 0.008
510	0.006 ± 0.005	0.005 ± 0.004	0.020 ± 0.006	0.005 ± 0.005
555	0.002 ± 0.002	0.002 ± 0.001	0.007 ± 0.002	0.001 ± 0.001
665	0.004 ± 0.004	0.004 ± 0.004	0.012 ± 0.004	0.004 ± 0.004
676	0.006 ± 0.005	0.005 ± 0.004	0.016 ± 0.005	0.004 ± 0.004

Table 3
Attenuated light in a PAR region in the upper 10 m layer of the water column (compared to surface PAR levels), integrated (0–10 m) PAR diffuse attenuation coefficients (K_d), depths of 10% and 1% (euphotic zone for PAR or 1% penetration depth for UV) of irradiance levels relative to the surface under different light conditions (clear sky and overcast). Same values are presented for the wavelength 355 nm (integrated over 350–360 nm) for clear sky conditions. PuW — is pure water constituent, PuW, CDOM — pure water and CDOM, PuW, part — pure water and particles, total — is total attenuation by pure water, CDOM and particles. Calculations are made at noon on September 15th for the layer 0–50 m.

	Fraction of light attenuated at 10 m		K_d (0–10 m)		$Z_{10\%}$ (m)		$Z_{1\%}$ (m)	
	EGC	WSC	EGC	WSC	EGC	WSC	EGC	WSC
PAR, clear sky conditions, 15 September								
PuW	0.61		0.09		>50		>50	
PuW, CDOM	0.83	0.76	0.18	0.15	14.6	19.0	34.1	46.1
PuW, part	0.63	0.81	0.10	0.17	34.3	15.5	>50	37.5
Total	0.84	0.81	0.18	0.17	14.0	15.5	31.5	37.4
PAR, overcast conditions, 15 September								
PuW	0.60		0.08		>50		>50	
PuW, CDOM	0.80	0.74	0.16	0.13	16.6	21.3	38.4	>50
PuW, part	0.62	0.78	0.09	0.15	37.6	17.7	>50	42.0
Total	0.81	0.78	0.17	0.15	15.8	17.7	35.4	41.9
355 nm (averaged over 350–360 nm), clear sky conditions, 15 September								
PuW	0.28		0.03		>50		>50	
PuW, CDOM	0.99	0.92	0.48	0.25	4.7	9.1	9.7	17.9
PuW, part	0.32	0.93	0.04	0.27	46.2	8.4	>50	16.8
Total	0.99	0.93	0.48	0.27	4.6	8.4	9.6	16.7

Differences in $a_p(440)$ between EGC and WSC may be caused by contrasting environmental factors such as stratification, sea ice distribution, and nutrient availability (Cherkasheva et al., 2014; Hop et al., 2006). Most likely, the major factor is sea-ice extent and area, potentially damping primary productivity through light attenuation in the EGC compared to WSC. As a consequence, this results in a generally lower $a_p(440)$ in the EGC than in the WSC. Also, particulate absorption is more dependent on local productivity compared to CDOM, and therefore likely has a stronger seasonality. Highest chlorophyll-a concentrations in the northern Fram Strait are typically observed during May-July, with lower chlorophyll-a values in August (Cherkasheva et al., 2014). In their study, satellite-derived climatology of chlorophyll-a concentration in August for the period 1998–2009 is in agreement with our findings of higher $a_p(440)$ in the eastern side of the Fram Strait compared to the western side. Thus, one could bear in mind that the contribution of particulate absorption should be higher during summer and our synoptic transects in September can show a lower estimate of particulate absorption that can be found in the area at other times of year.

4.3. Relevance of $a_p(\lambda)$ and $a_{CDOM}(\lambda)$ to underwater light distribution

Calculations made with ECOLIGHT 5.4.1 show that pure water and CDOM are responsible for 83% and 76% of PAR attenuation in the uppermost 0–10 m in the EGC and WSC, respectively. These values are higher than those (73%) reported for the Barents Sea by Hancke et al. (2014) based on average CDOM absorption found in their study. Consequently, euphotic zone depths are estimated as 34.1 (EGC) and 46.1 m

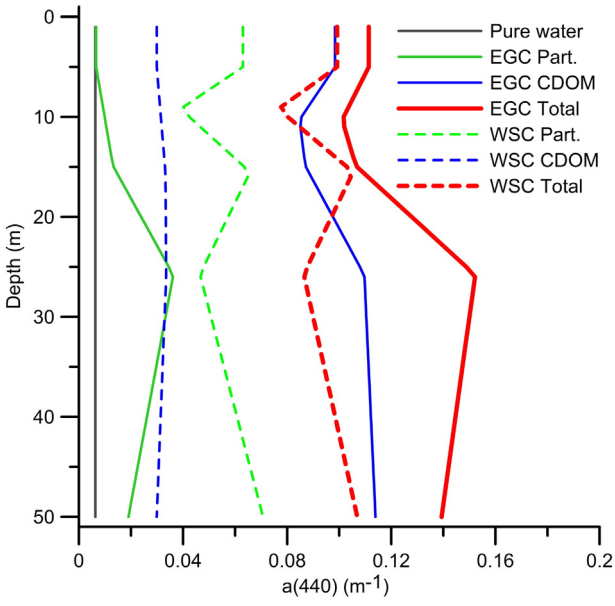

Fig. 6. Vertical profiles of absorption coefficient (λ = 440 nm) by pure water, CDOM and particles used in ECOLIGHT 5.1.4 model runs. (For interpretation of the references to color in this figure legend, the reader is referred to the web version of the article.)

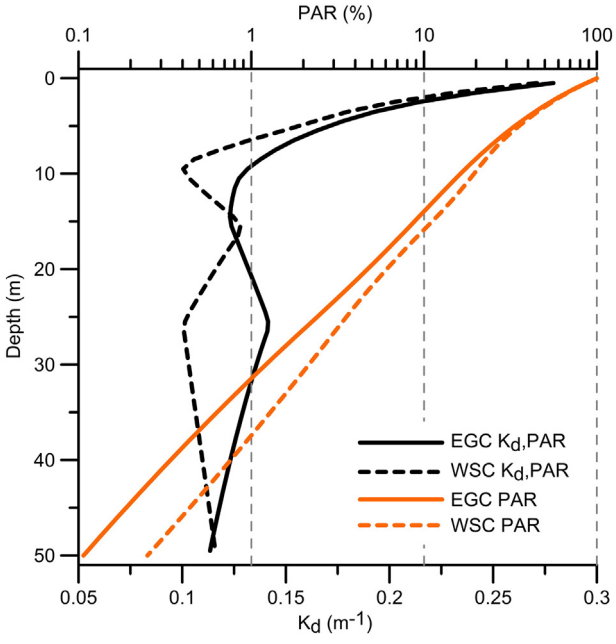

Fig. 7. Modeled vertical profiles of diffuse attenuation coefficients (K_d) in the EGC and WSC, and corresponding vertical profiles of PAR (logarithmic scale) in the absence of sea-ice. (For interpretation of the references to color in this figure legend, the reader is referred to the web version of the article.)

(WSC), which is lower compared to 55.5 m in the Barents Sea. Thus, when considering pure water and CDOM only, in both EGC and WSC light attenuation is higher than in the Barents Sea (Hancke et al., 2014). Pure water and particles account for 63% (EGC) and 81% (WSC) of the attenuated energy in top 10 m, which is comparable with model runs with 1 mg Chl a m^{-3} in Hancke et al. (2014) with a portion of attenuated light equal to 72%. Including all optically active components (pure water, CDOM and particles) results in 84% (EGC) and 81% (WSC) of attenuated energy in the upper 10 m, which is higher compared to the Barents Sea study with average CDOM absorption and 1 mg Chl a m^{-3} (80%).

Results from our modeling exercise are in line with information on CDOM and particulate absorption discussed in Sections 4.1. and 4.2. We found that CDOM is a primary contributor to PAR attenuation in the EGC waters whereas particles are a major contributor to PAR attenuation in the WSC area. Importance of CDOM absorption to the total absorption budget in various regions of the Arctic Ocean has been previously highlighted by Pegau (2002), Granskog et al. (2007), and Hill (2008). However, when considering effect of both CDOM and particles, PAR attenuation in the upper 10 m is only slightly higher in the EGC than in WSC. Here, it is important to mention that K_d in the PAR region also accounts for absorption by water itself. Given high absorption by pure water at longer wavelengths (>550–600 nm) within the PAR range (Pope and Fry, 1997), similarity in K_d in the uppermost 5–6 m seen in Fig. 7 can be partially explained the contribution of pure water absorption.

Differences between EGC and WSC are more pronounced when looking at the ultraviolet region of the solar spectrum (355 nm). In the EGC waters, 99% of the irradiance at 355 nm is attenuated in the upper 10 m, compared to only 93% in the WSC. Corresponding euphotic depths are 9.6 m for EGC and 16.7 m for WSC.

While some UV light can be utilized by photosynthetic organisms, it is known to be responsible for a large part of the photoinhibition of photosynthesis in aquatic systems (e.g. Kirk, 1994). The amount of UV solar radiation reaching sea-ice and ocean surface largely depends on ozone concentrations in the atmosphere (e.g., Nicolet, 1975). While there has been recent reports on stratospheric ozone depletions in the Arctic (Manney et al., 2011), generally, stratospheric ozone has been recovering over the past decades and this trend is expected to continue in the future (Coldewey-Egbers et al., 2014). Hamre et al. (2008) showed that depletion in stratospheric ozone indeed results in elevated UV in sea-ice covered and open Polar waters; however it also results in increased PAR levels compensating negative effects of UV with overall minor effect on primary productivity, hence on optical properties influenced by particulate absorption and scattering. Therefore, it is unlikely that changes in stratospheric ozone as an external factor would play an important role for optical properties of seawater and marine ecosystem.

Changes in optical properties in the WSC area in the future may potentially be associated with the dynamics and seasonality of phytoplankton, that is in turn, depends on oceanographic and sea-ice conditions. Given the absence or low concentrations (mostly over the West Spitsbergen Shelf) of sea-ice in the WSC area, it is difficult to expect that substantial changes might occur with respect to seawater optical properties. Hydrographic conditions in this region as well as in a central Fram Strait are known for high spatial and temporal variability (Johannessen et al., 1987; Tverberg and Nøst, 2009), and to a large extent, changes in optical properties (mostly particulate absorption) will be driven by this variability.

In the EGC, more drastic changes may be expected. Sea-ice is currently covering large areas in the region of EGC year-around, limiting the euphotic depth. However, if recent sea-ice thinning trends in the Fram Strait (Hansen et al., 2013; Renner et al., 2014) and in the Arctic Ocean proper (e.g. Meier et al., 2014) proceed in the future, one might expect CDOM to become more important for the absorption budget of the upper ocean. Thinning of the sea-ice cover would result in higher PAR availability in the surface ocean and thus potentially higher productivity, which is in line with recent findings from the Central Arctic (Arrigo et al., 2008) as well as in the central Fram Strait (Cherkasheva et al., 2014). However, the response of phytoplankton to increased light levels is a complex interplay between light, temperature, nutrient availability, stratification and light-adaptation and acclimation of the phytoplankton themselves (e.g. Palmer et al., 2013), and thus not only dependent on changes in light availability. When sea ice is present, as currently is the case, euphotic depths will be obviously even shallower in the EGC, than presented here. Further, sea-ice meltwaters will generally result in a shallow pycnocline, with the potential for subsurface chl a maxima (SCMs), at rather shallow depths without harmful UV radiation. SCMs are prevalent features in the in the Arctic Ocean and important for integrated primary production estimates (Ardyna et al., 2013). On the other hand Bélanger et al. (2013) reported that melting sea ice released material that slightly reduced the amount of PAR, although we did not observe this in the EGC. Increased primary productivity, however, would alter optical properties of surface waters in the EGC by increasing light attenuation by particulate matter.

5. Conclusions

There are significant differences in the spectral absorption properties of CDOM and particles between the Polar waters of the East Greenland Current and the Atlantic waters of the West Spitsbergen Current. Highest CDOM absorption is associated with the core of the PW in the EGC, while lowest CDOM absorption is found in the WSC area. In contrast, particulate absorption is greatest in the WSC. We expect that the contrast in particulate absorption would be even higher in spring and summer as indicated by chlorophyll distribution in the Fram Strait (Cherkasheva et al., 2014).

CDOM absorption levels found in AW in the Fram Strait are similar to those found in the Barents Sea. However, CDOM absorption in PW in the EGC area is consistent with previous studies in the Arctic Ocean proper and is more than 3 times higher than CDOM absorption levels found in Arctic waters of the Barents Sea (Hancke et al., 2014); this points towards the fact that waters in the northern Barents Sea are likely recirculated Atlantic water, rather than true Polar waters, and optical properties are dominated by phytoplankton.

Despite a contrast in optical properties between EGC and WSC, PAR attenuation in the upper 10 m is only slightly higher in the EGC than in WSC. UV attenuation is much stronger in EGC waters compared to WSC. With future sea ice cover changes expected in the Fram Strait and the Arctic Ocean, seawater optical properties in the EGC area will become more important in shaping the underwater light regime. In this regard, western side of the Fram Strait might serve as a good case study region with true Polar waters outflow to unveil consequences of sea-ice decrease in the Arctic Ocean proper on biogeochemical and biological processes, such as photo-oxidation of organic matter, nutrient mineralization, and primary productivity of phytoplankton and sea-ice algae. The described optical contrasts between the optically complex waters in the EGC and algal-dominated waters in the WSC call for further efforts on development of regional remote sensing ocean color algorithms and their ground truthing. Future studies will also be needed in order to resolve seasonal variability of optical properties, especially the contribution of phytoplankton, and its implications for marine ecosystems and the energy budget of waters in the Fram Strait.

Acknowledgements

We thank the crew of R.V. Lance and colleagues for the help with collecting samples onboard. We thank Olga Pavlova for providing sea-ice data for the period of observations and Paul Dodd for the preparation of the CTD data set and helpful comments. We thank Philipp Assmy for a helpful discussion. A.K.P., M.A.G., S.R.H. and S.F.P. were supported by the Centre for Ice, Climate and Ecosystems (ICE) at the Norwegian Polar

Institute. A.K.P. was partially supported by the joint Russian–Norwegian (AARI-NPI) FRAM Arctic Climate Research Laboratory fellowship, the Research Council of Norway's Yggdrasil program 2010-11 (grant no. 202423/V11), A.K.P. and B.V.I. by the Russian Foundation for Basic Research (RFBR), research project 12-05-00780_a and 14-05-10065, Roshydromet project 1.5.3.3, and President Grant MK-4049.2014.8. A.K.P., M.A.G. and S.R.H. research work has partially received funding from the Polish–Norwegian Research Programme operated by the National Centre for Research and Development under the Norwegian Financial Mechanism 2009–2014 in the frame of Project Contract Pol-Nor/197511/40/2013, CDOM-HEAT. C.A.S. was supported by Danish Strategic Research Council to the research project NAACOS (grant 10-093903). Article preparation and publication were supported by the Research Council of Norway through the STASIS project (221961/F20).

References

AMAP, 2011. Snow, Water, Ice and Permafrost in the Arctic (SWIPA). Oslo: Arctic Monitoring and Assessment Programme (AMAP), Oslo, Norway.

Amon, R.M.W., 2003. The role of dissolved organic matter for the organic carbon cycle in the Arctic Ocean. In: Stein, R., MacDonald, R. (Eds.), The Organic Carbon Cycle in the Arctic Ocean. Springer, Berlin, pp. 83–99.

Ardyna, M., Babin, M., Gosselin, M., Devred, E., Bélanger, S., Matsuoka, A., Tremblay, J.-É., 2013. Parameterization of vertical chlorophyll a in the Arctic Ocean: impact of the subsurface chlorophyll maximum on regional, seasonal, and annual primary production estimates. Biogeosciences 10, 4383–4404. http://dx.doi.org/10.5194/bg-10-4383-2013.

Arrigo, K.R., van Dijken, G., Pabi, S., 2008. Impact of a shrinking Arctic ice cover on marine primary production. Geophys. Res. Lett. 35 (19).

Bélanger, S., Cizmeli, S.A., Ehn, J., Matsuoka, A., Doxaran, D., Hooker, S., Babin, M., 2013. Light absorption and partitioning in Arctic Ocean surface waters: impact of multiyear ice melting. Biogeosciences 10, 6433–6452. http://dx.doi.org/10.5194/bg-10-6433-2013.

Belzile, C., Johannessen, S.C., Gosselin, M., Demers, S., Miller, W.L., 2000. Ultraviolet attenuation by dissolved and particulate constituents of first-year ice during late spring in an Arctic polynya. Limnol. Oceanogr. 45 (6), 1265–1273.

Bricaud, A., Stramski, D., 1990. Spectral absorption coefficients of living phytoplankton and nonalgal biogenous matter: a comparison between the Peru upwelling area and Sargasso Sea. Limnol. Oceanogr. 35, 562–582.

Cherkasheva, A., Bracher, A., Melsheimer, C., Köberle, C., Gerdes, R., Nöthig, E.M., Boetius, A., 2014. Influence of the physical environment on polar phytoplankton blooms: a case study in the Fram Strait. J. Mar. Syst. 132, 196–207.

Coldewey-Egbers, M., Loyola, R., Diego, G., Braesicke, P., Dameris, M., Roozendael, M., Zimmer, W., 2014. A new health check of the ozone layer at global and regional scales. Geophys. Res. Lett. 41, 4363–4372. http://dx.doi.org/10.1002/2014GL060212.

Dodd, P.A., Rabe, B., Hansen, E., Falck, E., Mackensen, A., Rohling, E., Kristiansen, S., 2012. The freshwater composition of the Fram Strait outflow derived from a decade of tracer measurements. J. Geophys. Res. Oceans 117 (C11).

Falk-Petersen, S., Hop, H., Budgell, W.P., Hegseth, E.N., Korsnes, R., Løyning, T.B., Ørbæk, J.B., Kawamura, T., Shirasawa, K., 2000. Physical and ecological processes in the marginal ice zone of the northern Barents Sea during the summer melt period. J. Mar. Syst. 27 (1), 131–159.

Granskog, M.A., 2012. Changes in spectral slopes of colored dissolved organic matter absorption with mixing and removal in a terrestrially dominated marine system (Hudson Bay, Canada). Mar. Chem. 134, 10–17. http://dx.doi.org/10.1016/j.marchem.2012.02.008.

Granskog, M.A., Macdonald, R.W., Mundy, C.-J., Barber, D.G., 2007. Distribution, characteristics and potential impacts of chromophoric dissolved organic matter (CDOM) in the Hudson Strait and the Hudson Bay, Canada. Cont. Shelf Res. 27 (15). http://dx.doi.org/10.1016/j.csr.2007.05.001.

Granskog, M.A., Stedmon, C.A., Dodd, P.A., Amon, R.M., Pavlov, A.K., Steur, L., Hansen, E., 2012. Characteristics of colored dissolved organic matter (CDOM) in the Arctic outflow in the Fram Strait: assessing the changes and fate of terrigenous CDOM in the Arctic Ocean. J. Geophys. Res. Oceans 117 (C12).

Hamre, B., Stamnes, J.J., Frette, O., Erga, S.R., Stamnes, K., 2008. Could stratospheric ozone depletion lead to enhanced aquatic primary production in the polar regions? Limnol. Oceanogr. 53 (1), 332–338.

Hancke, K., Hovland, E.K., Volent, Z., Pettersen, R., Johnsen, G., Moline, M., Sakshaug, E., 2014. Optical properties of CDOM across the Polar Front in the Barents Sea: origin, distribution and significance. J. Mar. Syst. 130, 219–227.

Hansen, E., Gerland, S., Granskog, M.A., Pavlova, O., Renner, A.H.H., Haapala, J., Tschudi, M., 2013. Thinning of Arctic sea-ice observed in Fram Strait: 1990–2011. J. Geophys. Res. Oceans 118 (10), 5202–5221. http://dx.doi.org/10.1002/jgrc.20393.

Hill, V.J., 2008. Impacts of chromophoric dissolved organic material on surface ocean heating in the Chukchi Sea. J. Geophys. Res. Oceans 113 (C7). http://dx.doi.org/10.1029/2007JC004119.

Hop, H., Falk-Petersen, S., Svendsen, H., Kwasniewski, S., Pavlov, V., Pavlova, O., Soreide, J.E., 2006. Physical and biological characteristics of the pelagic system across Fram Strait to Kongsfjorden. Prog. Oceanogr. 71, 182–231. http://dx.doi.org/10.1016/j.pocean.2006.09.007.

Hudson, S.R., Granskog, M.A., Sundfjord, A., Randelhoff, A., Renner, A.H., Divine, D.V., 2013. Energy budget of first-year Arctic sea ice in advanced stages of melt. Geophys. Res. Lett. 40 (11), 2679–2683. http://dx.doi.org/10.1002/grl.50517.

Jackson, J.M., Carmack, E.C., McLaughlin, F.A., Allen, S.E., Ingram, R.G., 2010. Identification, characterization, and change of the near-surface temperature maximum in the Canada Basin, 1993–2008. J. Geophys. Res. 115. http://dx.doi.org/10.1029/2009JC005265 C05021.

Johannessen, J.A., Johannessen, O.M., Svendsen, E., Shuchman, R., Manley, T., Campbell, W.J., Van Leer, J., 1987. Mesoscale eddies in the Fram Strait marginal ice zone during the 1983 and 1984 Marginal Ice Zone Experiments. J. Geophys. Res. Oceans 92 (C7), 6754–6772.

Kirk, J.T.O., 1994. Light and Photosynthesis in Aquatic Ecosystems. Cambridge University Press.

Kolber, Z., Falkowski, P.G., 1993. Use of active fluorescence to estimate phytoplankton photosynthesis in situ. Limnol. Oceanogr. 38 (8), 1646–1665.

Loisel, H., Morel, A., 1998. Light scattering and chlorophyll concentration in case 1 waters: a reexamination. Limnol. Oceanogr. 43 (5), 847–858.

Manney, G.L., Santee, M.L., Rex, M., Livesey, N.J., Pitts, M.C., Veefkind, P., Zinoviev, N.S., 2011. Unprecedented Arctic ozone loss in 2011. Nature 478 (7370), 469–475.

Matsuoka, A., Huot, Y., Shimada, K., Saitoh, S.I., Babin, M., 2007. Bio-optical characteristics of the western Arctic Ocean: implications for ocean color algorithms. Can. J. Remote. Sens. 33 (6), 503–518.

Matsuoka, A., Hill, V., Huot, Y., Babin, M., Bricaud, A., 2011. Seasonal variability in the light absorption properties of western Arctic waters: parameterization of the individual components of absorption for ocean color applications. J. Geophys. Res. Oceans 116 (C2).

Matsuoka, A., Babin, M., Doxaran, D., Hooker, S.B., Mitchell, B.G., Bélanger, S., Bricaud, A., 2014. A synthesis of light absorption properties of the Arctic Ocean: application to semianalytical estimates of dissolved organic carbon concentrations from space. Biogeosciences 11, 3131–3147.

Meier, W.N., Hovelsrud, G.K., Oort, B.E., Key, J.R., Kovacs, K.M., Michel, C., Haas, C., Granskog, M.A., Gerland, S., Perovich, D.K., Makshtas, A., Reist, J.D., 2014. Arctic sea-ice in transformation: a review of recent observed changes and impacts on biology and human activity. Rev. Geophys. 115. http://dx.doi.org/10.1002/2013RG000431.

Mitchell, B.G., 1990. Algorithms for determining the absorption coefficient for aquatic particulates using the quantitative filter technique. In Orlando'90, 16–20 April. International Society for Optics and Photonics, pp. 137–148.

Mobley, C.D., 1994. Light and water. Radiative transfer in natural waters. Academic Press., San Diego.

Mobley, C.D., Sundman, L.K., 2008. Hydrolight 5 Ecolight 5 Technical Documentation. Sequoia Scientific, Incorporated, Bellevue, WA, 98005, p. 95.

Nicolaus, M., Katlein, C., Maslanik, J., Hendricks, S., 2012. Changes in Arctic sea ice result in increasing light transmittance and absorption. Geophys. Res. Lett. 39 (24).

Nicolet, M., 1975. Stratospheric ozone: an introduction to its study. Rev. Geophys. 13 (5), 593–636.

Palmer, M.A., van Dijken, G.L., Mitchell, B.G., Seegers, B.J., Lowry, K.E., Mills, M.M., Arrigo, K.R., 2013. Light and nutrient control of photosynthesis in natural phytoplankton populations from the Chukchi and Beaufort seas, Arctic Ocean. Limnol. Oceanogr. 58 (6), 2185–2205.

Pavlov, A.K., Tverberg, V., Ivanov, B.V., Nilsen, F., Falk-Petersen, S., Granskog, M.A., 2013. Warming of Atlantic Water in two west Spitsbergen fjords over the last century (1912-2009). Polar Res. 32, 11206. http://dx.doi.org/10.3402/polar.v32i0.11206.

Pegau, W.S., 2002. Inherent optical properties of the Central Arctic surface waters. J. Geophys. Res. 107, 8035. http://dx.doi.org/10.1029/2000JC000382.

Perovich, D., Richter-Menge,, J., Polashenski, C., Elder, B., Arbetter, T., Brennick, O., 2014. Sea-ice mass balance observations from the North Pole Environmental Observatory. Geophys. Res. Lett. 41 (6), 2019–2025.

Polyakov, I.V., Beszczynska, A., Carmack, E.C., Dmitrenko, I.A., Fahrbach, E., Frolov, I.E., Walsh, J.E., 2005. One more step toward a warmer Arctic. Geophys. Res. Lett. 32 (17).

Polyakov, I.V., Alexeev, V.A., Ashik, I.M., Bacon, S., Beszczynska-Möller, A., Carmack, E.C., Woodgate, R., 2011. Fate of early 2000s Arctic warm water pulse. Bull. Am. Meteorol. Soc. 92 (5), 561–566.

Pope, R.M., Fry, E.S., 1997. Absorption spectrum (380–700 nm) of pure water. II. Integrating cavity measurements. Appl. Opt. 36, 8710–8723.

Popova, E.E., Yool, A., Coward, A.C., Dupont, F., Deal, C., Elliott, S., Zhang, J., 2012. What controls primary production in the Arctic Ocean? Results from an intercomparison of five general circulation models with biogeochemistry. J. Geophys. Res. Oceans 117 (C8).

Post, E., Bhatt, U.S., Bitz, C.M., Brodie, J.F., Fulton, T.L., Hebblewhite, M., Walker, D.A., 2013. Ecological consequences of sea-ice decline. Science 341 (6145), 519–524.

Renner, A.H., Gerland, S., Haas, C., Spreen, G., Beckers, J.F., Hansen, E., Goodwin, H., 2014. Evidence of Arctic sea-ice thinning from direct observations. Geophys. Res. Lett. 41, 5029–5036. http://dx.doi.org/10.1002/2014GL060369.

Saloranta, T.M., Svendsen, H., 2001. Across the Arctic front west of Spitsbergen: high-resolution CTD sections from 1998–2000. Polar Res. 20 (2), 177–184.

Scully, N.M., Miller, W.L., 2000. Spatial and temporal dynamics of colored dissolved organic matter in the north water polynya. Geophys. Res. Lett. 27 (7), 1009–1011.

Serreze, M.C., Barry, R.G., 2011. Processes and impacts of Arctic amplification: a research synthesis. Glob. Planet. Chang. 77 (1), 85–96.

Smith, R.C., 1973. Optical properties of the Arctic upper water. Arctic 303–313.

Smith, W.O., Baumann, M.E., Wilson, D.L., Aletsee, L., 1987. Phytoplankton biomass and productivity in the marginal ice zone of the Fram Strait during summer 1984. J. Geophys. Res. Oceans 92 (C7), 6777–6786.

Staehr, P.A., Markager, S., 2004. Parameterization of the chlorophyll a-specific in vivo light absorption coefficient covering estuarine, coastal and oceanic waters. Int. J. Remote Sens. 25 (No. 22), 5117–5130.

Stedmon, C.A., Markager, S., 2001. The optics of chromophoric dissolved organic matter (CDOM) in the Greenland Sea: an algorithm for differentiation between marine and terrestrially derived organic matter. Limnol. Oceanogr. 46 (8), 2087–2093.
Stedmon, C.A., Amon, R.M.W., Rinehart, A.J., Walker, S.A., 2011. The supply and characteristics of colored dissolved organic matter (CDOM) in the Arctic Ocean: Pan Arctic trends and differences. Mar. Chem. 124 (1), 108–118.
Stocker, T.F., Qin, D., Plattner, G.K., Tignor, M., Allen, S.K., Boschung, J., Midgley, P.M., 2013. Climate change 2013: the physical science basis. Intergovernmental Panel on Climate Change, Working Group I Contribution to the IPCC Fifth Assessment Report (AR5). Cambridge Univ Press, New York.
Sverdrup, H.U., Johnson, M.W., Fleming, R.H., 1942. The Oceans: Their Physics, Chemistry, and General Biology Vol. 1087. Prentice-Hall, New York.
Swift, J.H., Aagaard, K., 1981. Seasonal transitions and water mass formation in the Iceland and Greenland seas. Deep-Sea Res. 28A, 1107–1129.
Taylor, J.R., Ferrari, R., 2011. Ocean fronts trigger high latitude phytoplankton blooms. Geophys. Res. Lett. 38 (23).
Tverberg, V., Nøst, O.A., 2009. Eddy overturning across a shelf edge front: Kongsfjorden, west Spitsbergen. J. Geophys. Res. Oceans 114 (C4).
U.S. Department of Commerce, National Oceanic and Atmospheric Administration, National Geophysical Data Center, 2006. 2-minute Gridded Global Relief Data (ETOPO2v2). Natl. Geophys. Data Cent, Boulder, Colo (http://www.ngdc.noaa.gov/mgg/fliers/06mgg01.html).
Vancoppenolle, M., Bopp, L., Madec, G., Dunne, J., Ilyina, T., Halloran, P.R., Steiner, N., 2013. Future Arctic Ocean primary productivity from CMIP5 simulations: uncertain outcome, but consistent mechanisms. Glob. Biogeochem. Cycles 27 (3), 605–619.
Walczowski, W., Piechura, J., Goszczko, I., Wieczorek, P., 2012. Changes in Atlantic water properties: an important factor in the European Arctic marine climate. ICES J. Mar. Sci. 69 (5), 864–869.
Wang, C., Granskog, M.A., Gerland, S., Hudson, S.R., Perovich, D.K., Nicolaus, M., Bratrein, M., 2014. Autonomous observations of solar energy partitioning in first-year sea-ice in the Arctic Basin. J. Geophys. Res. Oceans 119 (3), 2066–2080. http://dx.doi.org/10.1002/2013JC009459.
Wassmann, P., Duarte, C.M., Agusti, S., Sejr, M.K., 2011. Footprints of climate change in the Arctic marine ecosystem. Glob. Chang. Biol. 17 (2), 1235–1249.
Xie, H., Gosselin, M., 2005. Photoproduction of carbon monoxide in first-year sea ice in Franklin Bay, southeastern Beaufort Sea. Geophys. Res. Lett. 32 (12).
Xie, H., Aubry, C., Zhang, Y., Song, G., 2014. Chromophoric dissolved organic matter (CDOM) in first-year sea ice in the western Canadian Arctic. Mar. Chem. 165, 25–35. http://dx.doi.org/10.1016/j.marchem.2014.07.007.